A nonlinear autopilot for a piloted Quad-plane

D. A. Martínez-Velasco*, M. A. Martínez-Ramírez*, and H. Rodríguez-Cortés†
*Centro de Investigación y de Estudios Avanzados
del Instituto Politécnico Nacional,
Sección de Mecatrónica, Depto. de Ingeniería Eléctrica,
Ciudad de México, 07360, México
†Instituto Tecnológico Autónomo de México,
Campus Río Hondo, Departamento de Ingeniería Eléctrica y Electrónica,
Río Hondo 1, Ciudad de México, 01080, México

Abstract

Europe expects to realize urban air mobility (UAM) in five years. The initial commercial flights may require an onboard pilot, but eventually, the operations will be fully autonomous. Hybrid aerial vehicles that combine fixed and rotary wing capabilities, such as the Quad-plane, are emerging as the leading option for UAM. The Quad-plane combines a quadrotor with a fixed-wing configuration. This article proposes a nonlinear autopilot to simplify the pilot workload in different phases of the aircraft flight envelope. The nonlinear autopilot combines various nonlinear control techniques integrated using a state machine. During take-off and landing, in a quadrotor configuration, the pilot controls the aircraft's Cartesian position while the autopilot stabilizes the attitude and height. The autopilot also manages the transitions from quadrotor to fixed-wing aircraft and vice versa. While operating as a fixed-wing aircraft, the auto- pilot commands the aircraft's aerodynamic speed, the flight path angle, and the lateral dynamic. The autopilot's performance is evaluated using Software in the Loop (STIL) with a co-simulation with MATLAB-Simulink and the X-Plane flight simulator.

1 Introduction

In recent years, passenger transportation in metropolitan areas has demanded solutions that increase the quality of life and satisfy ecological constraints. The current technological improvements in electrical propulsion, digitalized air traffic control, and flight control architectures are enabling the potential introduction of electric vehicles that combine vertical take-off and landing capabilities with the advantages of fixed-wing configurations to propose innovative and sustainable urban air mobility solutions [1, 2].

The two most prevalent aircraft configurations in aircraft design are the fixed-wing and rotary-wing configurations; their advantages and disadvantages are well-studied and known. Fixed-wing configurations boast higher cruise speed, endurance, and range than their counterparts. Additionally, they can carry heavier payloads. However, the main drawback lies in the fact that fixed-wing aircraft need a runway for take-off and landing, posing a significant challenge for urban air mobility solutions. On the other hand, rotatory-wing aircraft have vertical take-off and landing capabilities and the ability to hover. Nevertheless, they suffer from lower cruise speed, endurance, and range than their fixed-wing counterparts. Therefore, recently, aircraft designers have been exploring new configurations aiming to combine the advantages of both basic configurations, resulting in new conceptual designs such as hybrid aircraft.

The leading hybrid aircraft configurations are tail-sitter, tail-rotor, and tail-wing. In these configurations, the whole aircraft, the rotors, or the wing are rotated around the aircraft's lateral axis to align the power plant with the vertical or longitudinal axes according to the flight condition [3]. Recently, a new hybrid configuration, the Quad-plane, has been proposed. It is a straightforward combination of a quadrotor and a fixed-wing aircraft. The main difference between a Quad-plane and the other hybrid aircraft configurations, tail-sitter, tilt-rotor, and tilt-wing, is that the Quad-plane has a rotor dedicated to the fixed-wing aircraft configuration. As a result, the Quad-plane has redundant control inputs in some sectors of its flight envelope but is mechanically the simplest among the other hybrid configurations.

The Quad-plane configuration has a greater flight envelope, including VTOL capability and high cruise speeds; for that reason, this configuration has become an attractive alternative for multiple applications, whether

*E-mail: {dalexis.martinez,marcoa.martinez}@cinvestav.mx
†E-mail: hugo.rodriguez@itam.mx On sabbatical leave from Centro de Investigación y de Estudios Avanzados del Instituto Politécnico Nacional, Sección de Mecatrónica, Depto. de Ingeniería Eléctrica
** The second and third authors thank the support of Mexican CONAHCYT under project Ciencia de Frontera CF-2023-I-551

civil or military, and a strong contender to provide air urban mobility solutions. However, the tail-sitter aircraft from [4] has proved to be efficient in many civil applications.

Hybrid configurations have captured the scientific community's attention due to the complexity of the transition from one configuration to the other [5], [6]. During the transition, the aircraft has over-actuated degrees of freedom, requiring specific control inputs to avoid undesirable behavior. In particular, along the transition from fixed-wing to rotatory-wing configurations, it is essential that the control system for both configurations work in a coordinated way to avoid the wing's stall that could create a descending acceleration that the rotatory-wing configuration could not compensate for. Consequently, flight control design for Quad-planes is an active research subject. In reference [7], a robust nonlinear controller based on the incremental nonlinear dynamic inversion (INDI) approach so that the Quad-plane can follow a given path autonomously. The controller is complemented with reference models to the inner loops to shape the input commands and provide feedforward inputs. Numerical simulations are presented to evaluate the controller's performance. The work reported in [8] shows the design, dynamic modeling, and control synthesis for a QuadPlane. For each flight mode, there is a control algorithm; a four state hybrid automaton coordinates the transitions among the control algorithms. This control algorithm is validated through numerical simulations. In [9], a model-based nonlinear weight assignment principle and an active disturbance rejection control are proposed to improve the altitude control performance during the transition phase. The effectiveness of the aerodynamic model and controller is verified via simulations. In [10], based on the sliding mode control technique, an energy-effective altitude control law for a pusher-type QuadPlane UAV in transition phases is reported. The proposed control law estimates the aerodynamic forces along the longitudinal axis to optimize the required energy to hold the aircraft at a desired altitude. Simulation and actual flight test results show the proposed control performance. In [11], a super twisting sliding mode controller is designed to control the Quad-plane altitude during transition phases. The proposed algorithm is tested using actual UAV's aerodynamic parameters in the X-plane 11 simulation environment. In [12], a controller for all flight phases in a Quad-Plane is reported. The controller is based on the Incremental Nonlinear Control Allocation (INCA) technique. This controller avoids negative wing angles of attack, minimizing the loads on the rotors. Numerical simulations and experimental flights are presented to validate the algorithm. In [13], an observer-based optimal control approach for active combined fault and wind disturbance rejection for a Quad-plane. The control synthesis considers a linear model for the longitudinal plane and the transition modes. A numerical simulation demonstrates that for a typical Quad-plane flight profile at 100 m altitude, the observer-based wind gust and fault correction significantly enhance trajectory tracking performance.

Existing literature offers limited insights into the nonlinear nature of the Quad-plane dynamics and its full flight envelope. The framework presented in this study fills these gaps by designing the controllers considering the nonlinear Quad-plane model and covering a full flight mission from take-off to landing, going through the transition from quadrotor to fixed-wing aircraft and viceversa. This novel approach is a significant step toward understanding the Quad-plane capabilities.

Hence, this work introduces a nonlinear autopilot for different phases of a Quad-plane flight envelope, including the crucial transition from rotatory to fixed-wing configuration and vice versa. The autopilot is based on various control techniques and includes an exogenous disturbance estimator based on immersion and invariance [14]. For take-off and landing, the nonlinear autopilot commands the quadrotor attitude around the lateral and longitudinal axes, the angular speed around the vertical axis, and the height. The pilot controls the Cartesian position. For the transition mode from quadrotor to fixed-wing, the fixed-wing power plant accelerates the vehicle until the longitudinal speed is bigger than the wing stall speed; in this flight phase, the autopilot commands the vehicle's attitude using the auditor power plant. Once this condition on the longitudinal speed is satisfied, a longitudinal autopilot based on the Total Energy Control System approach commands the aircraft's aerodynamic speed. At the same time, the pilot can control the aircraft's translational position. This work is a direct continuation of the preliminary report in [15].

The outline of this report is as follows. Section 2 presents the QuadPlane dynamic model that will be taken into consideration for the control algorithms design. Section 3 addressed the control algorithms for each flight phase. Section 4 reports state machine that mixes each algorithm in order to achieve a smooth transition from pure mode flights. Section 5 presents the numerical simulation results obtained using the flight simulator X-Plane. This work ends at section 6 with some remarks and conclusions.

2 Quad-Plane dynamic model

The critical flight phase for a Quad-Plane aircraft happens at the transition from fixed-wing to rotatory-wing configurations and vice versa. Since the aircraft must hold a speed higher than the wing stall speed in a fixed-wing configuration, the transition's main features occur on the longitudinal plane. However, the whole

rotational dynamic must be considered since the lateral movements and rotation around the vertical axis must be kept bounded.

The Quad-plane model considered in this work is shown in Figure 1. The aircraft has four rotors as the power plant for the quadrotor configuration r_i, $i = 1, , 4$, and a fifth rotor r_5 for the fixed-wing configuration. Moreover, the vehicle has ailerons, elevators, and rudder for fixed-wing operation.

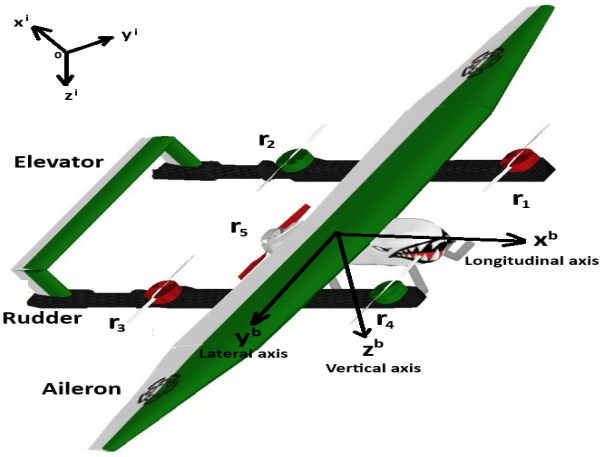

Figure 1: QuadPlane model. Body coordinated axis system $0x^by^bz^b$ and inertial coordinated axis system $0x^iy^iz^i$

The following differential equations describe the Quad-plane longitudinal translational dynamic model in mixed body and inertial coordinates [16]

$$\begin{aligned} \dot{z} &= -us_\theta + wc_\theta \\ m\dot{u} &= -mqw - mgs_\theta + \mathbf{q}SC_x + \kappa mg\delta_T \\ m\dot{w} &= mqu + mgc_\theta + \mathbf{q}SC_z - T_T \end{aligned} \tag{1}$$

with z the aircraft inertial position along the $0z^i$ inertial axis, u and w are the velocities along the $0x^b$ and $0z^b$ axes, respectievly. θ is the pitch angle, m the Quad-plane mass, q the pitch angular speed, g the gravity constant,

$$\mathbf{q} = \frac{1}{2}\rho(u^2 + w^2)$$

the dynamic pressure, with ρ the air density, S the Quad-plane wing surface. Moreover, $\delta_T \in (0, 1)$ the accelerator position for the fifth rotor, and $T_T = \sum_{i=1}^{4} T_i$ the total thrust generated by the quadrotor' rotors. Finally, C_x and C_z are the aerodynamic force coefficients.

The rotational dynamic model is given by

$$\begin{aligned} \dot{R} &= R\,\mathbf{S}(\Omega) \\ J\dot{\Omega} &= -\mathbf{S}(\Omega)J\Omega + M_P^b + M_Q^b \end{aligned} \tag{2}$$

with $R \in SO(3)$ the rotation matrix, with

$$SO(3) = \{R \in \mathbb{R}^{3\times3} | R^\top R = I, \det(R) = 1\}$$

The map $\mathbf{S}(\cdot) : \mathbb{R}^3 \to \mathfrak{so}(3)$, with $\mathfrak{so}(3)$ the Lie algebra of $SO(3)$, is defined as $a \times b = \mathbf{S}(a)b$ for all vectors $a, b \in \mathbb{R}^3$. Moreover, $\Omega = \begin{bmatrix} p & q & r \end{bmatrix}^\top$ is the angular velocity in the body coordinates, and

$$M_P^b = \mathbf{q}S \begin{bmatrix} b(C_l(\cdot) + C_{l_{\delta_a}}\delta_a + C_{l_{\delta_r}}\delta_r) \\ \bar{c}(C_m(\cdot) + C_{m_{\delta_e}}\delta_e) \\ b(C_n(\cdot) + C_{n_{\delta_a}}\delta_a + C_{n_{\delta_r}}\delta_r) \end{bmatrix}$$

are the aerodynamic moments[1] in fixed-wing configuration, where b is the wingspan, $C_l(\cdot)$ the roll aerodynamic moment coefficient, $C_{l_{\delta_a}}$ and $C_{l_{\delta_r}}$ the roll and yaw aerodynamic control coefficients, respectively, δ_a and δ_r the aileron and rudder deflection angles, respectively, $\bar{c}$ is the wing mean aerodynamic chord, $C_m(\cdot)$ the pitch aerodynamic moment coefficient, $C_{m_{\delta_e}}$ the pitch aerodynamic control coefficient, δ_e the elevator deflection angle, $C_n(\cdot)$ the yaw aerodynamic moment coefficient, $C_{n_{\delta_a}}$ and $C_{d_{\delta_r}}$ the roll and yaw aerodynamic control coefficients for yaw, respectively. Finally,

$$M_Q^b = \begin{bmatrix} M_{Q_p}^b \\ M_{Q_q}^b \\ M_{Q_r}^b \end{bmatrix} = \begin{bmatrix} l_1(T_1 + T_4 - T_3 - T_2) \\ l_2(T_1 + T_2 - T_3 - T_4) \\ Q_1 + Q_3 - Q_2 - Q_4 \end{bmatrix}$$

are the applied moments in quadrotor configuration with l_1 and l_2 the distances from the $0x^b$, $0y^b$ axes to the rotors' position. $T_i, i = 1, 2, 3, 4$ the thrust generated by each rotor and $Q_i, i = 1, 2, 3, 4$ the counter-rotating moment produced by each rotor.

Note that in both configurations, the rotational dynamic is fully actuated. However, the control moments from the aerodynamic surfaces are effective only after the Quad-plane aerodynamic speed is higher than the stall speed; below the wing stall speed, these aerodynamic moments act as disturbances for the quadrotor configuration. Conversely, the control inputs for the quadrotor configuration and the fifth rotor are available for the entire flight envelope.

3 Control Algorithms.

This section presents the control algorithms that are used during the transition phase from rotatory-wing to fixed-wing and vice versa. The control algorithms were developed using different control techniques and disturbances estimators making use of immersion and invariance.

[1] $(\cdot)$ represents the aerodynamic coefficients dependency on the aerodynamic angles, the angle of attack and the sideslip angle, the Reynolds number, and the angular velocity [16].

3.1 Attitude autopilot in quadrotor configuration (AAQC)

The attitude autopilot in quadrotor configuration works during take-off and landing procedures. Thus, the objective of this autopilot is to command the Quad-plane angular position around the lateral and longitudinal axes and the angular velocity around the vertical axis. The pilot can modify the angular and angular speed references to command the vehicle's position in the Cartesian plane.

The rotation matrix R is parameterized using the Tait-Bryan angles to design the AAQC autopilot

$$R = \begin{bmatrix} c_\theta c_\psi & s_\phi s_\theta c_\psi - c_\theta s_\psi & c_\phi s_\theta c_\psi + s_\theta s_\psi \\ c_\theta s_\psi & s_\phi s_\theta s_\psi + c_\theta c_\psi & c_\phi s_\theta s_\psi - s_\theta c_\psi \\ -s_\theta & c_\theta s_\phi & c_\theta c_\phi \end{bmatrix}$$

with ϕ the roll and yaw angles, respectively. By introducing the following notation for the columns of the matrix R

$$R = \begin{bmatrix} r_1^\top & r_2^\top & r_3^\top \end{bmatrix}$$

the first equation from (1) can be written in the following form [17]

$$\dot{r}_1 = r_1 \times \Omega, \quad \dot{r}_2 = r_2 \times \Omega, \quad \dot{r}_3 = r_3 \times \Omega$$

On the other hand, note that the gravity force acting on the vehicle expressed in body axes reads as

$$F_g^b = R^\top F_g^i = mgr_3$$

where $F_g^i = \begin{bmatrix} 0 & 0 & mg \end{bmatrix}^\top$. Hence, the AAQC objective is stated as follows: design control inputs M_Q^b to align the vector r_3 with $e_z = \begin{bmatrix} 0 & 0 & 1 \end{bmatrix}$ and to keep $r = 0$ for take off and landing and to $r_{3_d} = \begin{bmatrix} -s_{\theta_d} & c_{\theta_d} s_{\phi_d} & c_{\theta_d} c_{\phi_d} \end{bmatrix}$ and $r_d = 0$ for pilot commands.

The autopilot is designed following the nonlinear approach proposed in [18]. Thus, the attitude error is defined as $\tilde{r}_3 = r_3 \times r_{3_d}$. Then, one obtains

$$\dot{\tilde{r}}_3 = -\mathbf{S}(\Omega_d)\tilde{r}_3 - \mathbf{S}(r_{3_d})S(r_3)\tilde{\Omega} \tag{3}$$

with $\tilde{\Omega} = \Omega - \Omega_d$. Assuming that the references send by the pilot are piece wise constant, it is considered that $\dot{r}_{3_d} = 0$. The reference for the angular speed sent by the pilot is considered by defining $\Omega_d = \begin{bmatrix} 0 & 0 & r_d \end{bmatrix}^\top$.

The angular velocity error dynamic is described by

$$\begin{aligned} \dot{\tilde{\Omega}} &= J^{-1}\Big(-\mathbf{S}(\tilde{\Omega})J(\tilde{\Omega} + \Omega_d) - \mathbf{S}(\Omega_d)J\tilde{\Omega} \\ &\quad -\mathbf{S}(\Omega_d)J\tilde{\Omega}_d + M_P^b + M_Q^b\Big) \end{aligned} \tag{4}$$

with r_d assumed piece wise constant.

It is important to note that under low values of velocity, M_P^b takes values close to zero, so it can be considered a disturbance. Hence, for control design, the dynamic model (4) is expressed as

$$J\dot{\tilde{\Omega}} = -\mathbf{S}(\tilde{\Omega})J(\tilde{\Omega} + \Omega_d) - \mathbf{S}(\Omega_d)J\tilde{\Omega} + M_Q^b + \delta_M \tag{5}$$

with $\delta_M = -\mathbf{S}(\Omega_d)J\tilde{\Omega}_d + M_P^b$ modeling a disturbance with upper bounded first time derivative, this is, $||\dot{\delta}_M|| \leq k_0$ for some constant k_0.

The following controller is proposed

$$M_Q^b = -K_P\tilde{r}_3 - K_D\tilde{\Omega} - \hat{\delta}_M - \Gamma J\tilde{\Omega} \tag{6}$$

with K_P, K_D and Γ positive defined matrices. The error dynamics (3)-(5) in closed-loop with (6) reads as

$$\begin{aligned} \dot{\tilde{r}}_3 &= -S(\Omega_d)\tilde{r}_3 - S(r_{3_d})S(r_3)\tilde{\Omega} \\ J\dot{\tilde{\Omega}} &= -\mathbf{S}(\tilde{\Omega})J(\tilde{\Omega} + \Omega_d) - \mathbf{S}(\Omega_d)J\tilde{\Omega} - K_P\tilde{r}_3 \\ &\quad -K_D\tilde{\Omega} + \tilde{\delta}_M \\ \dot{\tilde{\delta}}_M &= -\Gamma\tilde{\delta}_M + \dot{\delta}_M \end{aligned} \tag{7}$$

where

$$\begin{aligned} \tilde{\delta}_M &= \delta_M - \hat{\delta}_M - \Gamma J\tilde{\Omega} \\ \dot{\tilde{\delta}}_M &= -\Gamma\Big(-\mathbf{S}(\tilde{\Omega})J(\tilde{\Omega} + \Omega_d) - \mathbf{S}(\Omega_d)J\tilde{\Omega} + \hat{\delta}_M \\ &\quad +\Gamma J\tilde{\Omega} + M_Q^b\Big) \end{aligned} \tag{8}$$

with $\tilde{M}$ the disturbance estimation error and $\hat{M}$ the state of the disturbance estimator.

3.2 Height Autopilot in Quadrotor Configuration (HAQC)

The HAQC aims to command the vehicle's height during take-off and landing operations without vertical speed measurements. The HAQC uses the quadrotor power plant to achieve this objective. For autopilot design, the following model is considered

$$\begin{aligned} \dot{\tilde{h}} &= -wc_\theta \\ \dot{w} &= gc_\theta - \tfrac{T_T}{m} + \delta_w \end{aligned} \tag{9}$$

with $\tilde{h} = h - h_d$ the heighterror, h the actual height and h_d the desired constant height. $\delta_w = qu + \mathbf{q}SC_z/m$ represents a disturbance. Once again, it is assumed that $|\dot{\delta}_z| \leq \kappa_1$ for some constant κ_1. The following control law is proposed

$$T_T = m(-k_p\tilde{h} + k_d(\hat{w} - \gamma_1\tilde{h}) - \gamma_2(\hat{w} - \gamma_1\tilde{h}) + \hat{\delta}_w) \tag{10}$$

where k_p, k_d, γ_1 and γ_2 are the autopilot gains, and

$$\begin{aligned} \dot{\hat{w}} &= gc_\theta + \hat{\delta}_w - \gamma_2(\hat{w} - \gamma_1\tilde{h}) - T_T/m \\ &\quad +\gamma_1(\hat{w} - \gamma_1\tilde{h})c_\theta \\ \dot{\hat{\delta}}_w &= \gamma_2(gc_\theta + \hat{\delta}_w - \gamma_2(\hat{w} - \gamma_1\tilde{h}) - T_T/m) \end{aligned} \tag{11}$$

where $\hat{w}$ is the vertical observer state, $\hat{\delta}_w$ is the state of the disturbance estimator. This observer/estimator is designed following the procedure reported in [19].

The system (9) in closed-loop with (10) and (11) is descrbed by

$$\begin{array}{rcl} \dot{\tilde{h}} & = & -wc_\theta \\ \dot{w} & = & k_p\tilde{h} - k_d w + k_d\tilde{w} + \tilde{\delta}_w \\ \dot{\tilde{w}} & = & \tilde{\delta}_w + \gamma_1\tilde{w}c_\theta \\ \dot{\tilde{\delta}}_w & = & -\gamma_1\gamma_2\tilde{w}c_\theta + \dot{\delta}_w \end{array} \tag{12}$$

where

$$\begin{array}{rcl} \tilde{w} & = & w - \hat{w} + \gamma_1\tilde{h} \\ \tilde{\delta}_w & = & \delta_w - \hat{\delta}_w + \gamma_2(\hat{w} - \gamma_1\tilde{h}) \end{array}$$

are the vertical speed observer and the estimation errors, respectively.

3.3 Longitudinal Velocity Autopilot in Quadrotor Configuration (LVAQC)

The LVAQC works only during the transition from quadrotor to fixed-wing. The desired velocity is set as the wing stall speed, and the fifth rotor is employed to attain it. In this flight state, the aircraft could accelerate longitudinally using the quadrotor power plant or the fifth rotor power. Here, it is proposed to use the fifth to accelerate longitudinally and to control the vehicle's attitude using the quadrotor power plant. The autopilot is designed considering the following dynamic model

$$\dot{u} = -gs_\theta + \kappa g\delta_T + \delta_u \tag{13}$$

where δ_T is the accelerator position for the fifth rotor and $\delta_u = qw + \mathbf{q}SC_x$ is considered as disturbance with upper bounded first time derivative. Thus, there exist κ_2 such that $|\delta_u| \leq \kappa_2$.

The following autopilot algorithm is proposed

$$\begin{array}{rcl} \delta_T & = & \frac{1}{\kappa g}(-k_{p_u}\tilde{u} + gs_\theta - \sigma_1 u - \hat{\delta}_u) \\ \dot{\hat{\delta}}_u & = & -\sigma_1(-gs_\theta + \sigma_1 u + \kappa g\delta_T + \hat{\delta}_u) \end{array} \tag{14}$$

with k_{p_u} and γ_1 autopilot positive gains, $\tilde{u} = u - u_d$ the longitudinal error speed, and u_d the reference speed equal to the wing stall speed. The closed-loop dynamics (13)-(14) reads as

$$\begin{array}{rcl} \dot{\tilde{u}} & = & -k_{p_u}\tilde{u} + \tilde{\delta}_u \\ \dot{\tilde{\delta}}_u & = & -\sigma_1\tilde{\delta}_u + \dot{\delta}_u \end{array} \tag{15}$$

3.4 Longitudinal Speed autopilot in fixed-wing configuration (LSAFC)

During the transition from fixed-wing to quadrotor, the aerodynamic speed must decrease to the wing stall speed. At this point, the autopilots AAQC and HAQC are activated. The following dynamic model is considered to design the autopilot engaged to decrease the aircraft's aerodynamic speed

$$\begin{array}{rcl} \frac{\dot{u}}{g} & = & -s_\theta + \kappa\delta_T + \frac{\delta_u}{g} \\ \dot{\theta} & = & q \\ \dot{q} & = & \mathbf{q}\frac{S\bar{c}}{I_{yy}}(C_m(\cdot) + C_{m_{\delta_e}}\delta_e) \end{array} \tag{16}$$

The following autopilot algorithm is proposed

$$\delta_T = \frac{1}{\kappa}\left(-\frac{\hat{\delta}_u + \sigma_1 u}{g} + \bar{\delta}_T\right) \tag{17}$$

with σ_2 a positive gain. Moreover,

$$\begin{array}{rcl} \bar{\delta}_T & = & \frac{1}{1+k_{p_h}}(k_{p_h}(2s_\theta + \frac{k_v}{g}\tilde{u}) + k_{i_h}\eta_1) \\ \dot{\eta}_1 & = & -\bar{\delta}_T + 2s_\theta + \frac{k_v}{g}\tilde{u} \end{array} \tag{18}$$

where k_{p_h}, k_{i_h} and k_v are positive constant gains, and

$$\begin{array}{rcl} \delta_e & = & -k_p s_\theta - k_d q + k_{p_l}(-\bar{\delta}_T + \frac{k_v}{g}\tilde{u}) + k_{i_l}\eta_2 \\ \dot{\eta}_2 & = & -\bar{\delta}_T + \frac{k_v}{g}\tilde{u} \end{array} \tag{19}$$

with k_p, k_d, k_{p_l}, and k_{i_l} positive constant gains. The closed-loop dynamic (16)-(19) is described by the following equations

$$\begin{array}{rcl} \frac{\dot{\tilde{u}}}{g} & = & \left(\frac{2k_{p_h}}{1+K_{p_h}} - 1\right)s_\theta + \frac{k_{p_h}}{1+k_{p_h}}\frac{k_v}{g}\tilde{u} + \frac{\tilde{\delta}_u}{g} \\ \dot{\theta} & = & q \\ \dot{q} & = & \mathbf{q}\frac{S\bar{c}}{I_{yy}}(C_m(\cdot) + C_{m_{\delta_e}}(-k_p s_\theta - k_d q \\ & & +k_{p_l}(-\bar{\delta}_T + \frac{k_v}{g}\tilde{u}) + k_{i_l}\eta_2)) \\ \dot{\eta}_1 & = & -\bar{\delta}_T + 2s_\theta + \frac{k_v}{g}\tilde{u} \\ \dot{\eta}_2 & = & -\bar{\delta}_T \\ \dot{\tilde{\delta}}_u & = & -\sigma_1\tilde{\delta}_u + \dot{\delta}_u \end{array} \tag{20}$$

It can be verified that if $\dot{\delta}_u = 0$ the only equilibrium point in (20) is $\tilde{u} = 0$. Using a linear approximation of the closed-loop dynamic in (20) the gains can be determined to prove local stability. The controller defined in (17)-(19) is based on the Total Energy Control described in [20] for the lineal case and [21] for the non-lineal case.

4 State Machine

This work proposes using a state machine with finite states to allow the pilot to switch among the proposed autopilots. The machine states are defined as [22]

$$\mathcal{Q} = \{\mathbf{LQM}, \mathbf{QM}, \mathbf{TQ2FW}, \mathbf{FWM}, \mathbf{TFW2Q}\}$$

with **LQM** landing in quadrotor configuration mode, **QM** quadrotor operation mode, including take-off,

TQ2FW transition from quadrotor to fixed-wing configurations, **FWM** fixed-wing operation mode, and **TFW2Q** transition from fixed-wing to quadrotor configurations. The automata's alphabet is defined by the binary position of two switches in the radio transmitter and a comparison between the actual longitudinal velocity and the wing stall longitudinal speed u_d. This is,

$$\sum = \{T_{11}, T_{12}, T_{21}, T_{22}, u > u_d, u < u_d/2\}$$

The machine states diagram in Figure 2 shows the different transitions for the pilot to operate the Quad-plane.

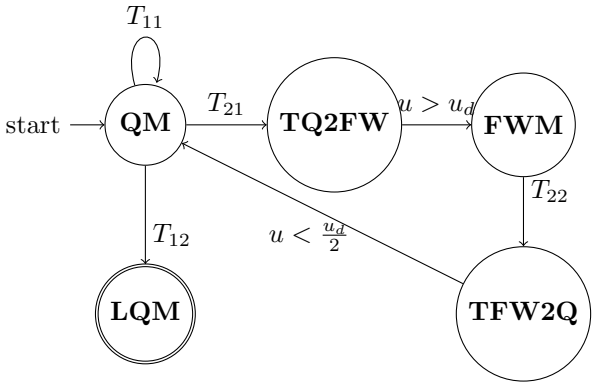

Figure 2: Machine states diagram.

Figure 3 shows the radio transmitter command configuration and the transition switches for take-off and landing. When the states **LQM** or **QM** are selected, *AAQC* controls the aircraft attitude, and the pilot can send roll and pitch angles and the yaw angular speed references; additionally, the *HAQC* regulates the aircraft's height. Once the pilot switches to state **TQ2FW**, the *AAQC*, *HAQC*, and *LVAQC* are active. The pilot can still send references for roll and pitch angles and the yaw angular speed commanded through M_Q^b, but its effectiveness decreases as u increases. In the state **FWM**, the pilot has complete control over the aircraft unless the pilot's thrust command is not giving enough power to reach a minimum speed above the wing stall speed; the LVAQC performs this task. During the **TFW2Q** state is active, the **LSAFC** commands the aircraft's longitudinal speed and the pitch angle. However, as u decreases, the control surfaces lose effectiveness. Hence, once the longitudinal speed is smaller than the wing stall speed, the *AAQC* and *HAQC* take control of the aircraft, and the pilot recovers authority on the vehicle's Cartesian position.

Figure 3: Stick and switch allocation on the transmitter

5 Numerical simulation results

A SITL co-simulation between MATLAB-Simulink and X-Plane [23] is reported to evaluate the autopilot. The X-Plane flight simulator solves the aircraft dynamic model through a simplified CFD (Computational Fluid Dynamic) analysis. The aircraft model was made using Plane-Maker, a software included in X-Plane. The aircraft's main features are reported in Table 1.

Parameter	Value	Parameter	Value
b	2.17m	S	1.32m
m	22.67kg	$\bar{c}$	0.45m
l_1	0.65m	l_2	0.8m

Table 1: Quad-plane physical parameters

The autopilot is evaluated using two simulations. The first considers optimal flight conditions; the second considers light turbulent conditions with wind speeds of about 11kt. In both simulations, the pilot takes off and moves in the Cartesian position in quadrotor mode. Then, the pilot moves the transition switch to the T_{22} position, and the aircraft reaches a longitudinal speed above the wing stall speed. The wing's stall speed was determined following the procedure reported in [24]. Once the state FWM is reached, the pilot has complete control over the aircraft. Then, the pilot selects the switch position T_{21} to start the transition from fixed-wing to quadrotor configuration. Finally, the switch position T_{11} is activated, and the aircraft begins the landing operation, this simulations can be seen at the following link https://youtu.be/c_qRoVBpvrA.

Mode	T_{1i}	T_{2i}
QM,TFW2Q	1	0
LQM	0	1/0
TQ2FW,FWM	1	1

Table 2: Binary channels and the flight modes

Figure 4 presents the binary channels′ evolution for the optimal flight conditions simulation. As was described before, the quadrotor takes off as soon as the simulation starts; this is commanded through T_{1i} (solid line) where $T_{11} = 1$ commands the take-off operation and $T_{12} = 0$ commands the landing operation and T_{2i} (segmented line) commands the transition from quadrotor to fixed-wing configuration through $T_{22} = 1$ and the inverse operation through $T_{21} = 0$, the mapping between the binary channels and the flight modes is displayed in Table 2. Figure 5 reports the angular moments calculated by the $AAQC$ around the $0x^b$ and $0y^b$ axes. As expected, these values only differ from zero when $u < u_d$.

Figure 6 shows the longitudinal speed u (left label), the aircraft's height time evolution h (right label), and the Quad-plane flying modes (blue line) in the no turbulence case. As observed, the autopilot ends the transition from quadrotor mode to fixed-wing mode once the aircraft reaches the stall speed (red line), and the transition from fixed-wing to quadrotor mode ends when the aircraft has a longitudinal speed lower than half the stall speed; this is possible since during this transition phase the residual wing's lift and the thrust generated by the rotors compensate the aircraft's weight.

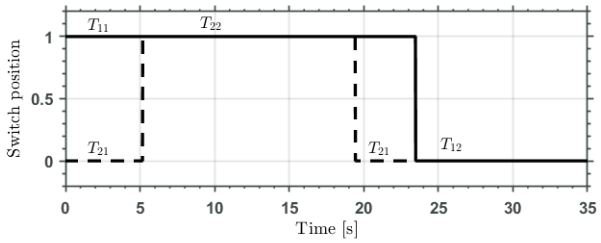

Figure 4: Binary channels evolution. The simulation with no turbulence.

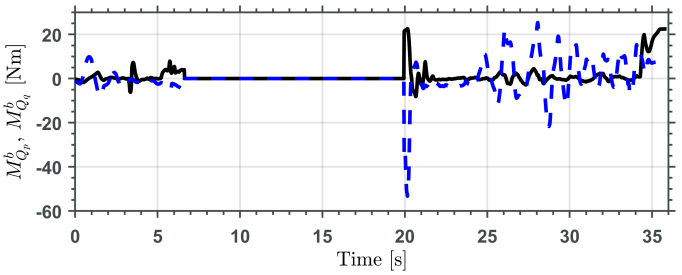

Figure 5: Angular moments computed by $AAQC$. The no turbulence simulation case.

Figure 7 presents the control moments M^b_p and M^b_q generated by the $AAQC$. In this case, these control moments reach higher values than in the previous simulation since the turbulent conditions disturb the aircraft.

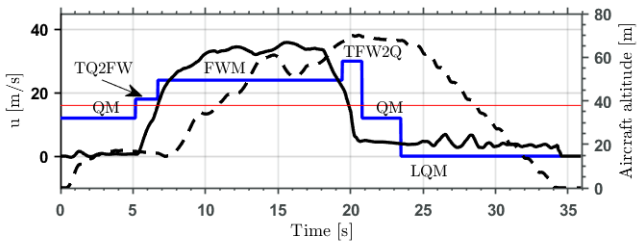

Figure 6: Quad-plane flight mission. Longitudinal speed u (continuos line) – and height h (dashed line). The no turbulence simulation case.

Figure 8 shows the longitudinal speed u (solid line, left label), the aircraft's height time evolution (dashed line, right label) and the Quad-plane transitions (blue line) with turbulence conditions. As a remark, the longitudinal velocity perturbation due to the turbulence conditions can be seen during the landing operation. Also, since the aircraft was flying against the wind, the resulting drag decelerated the vehicle, leading to a really short transition from fixed wing to quadrotor mode ($TFW2Q$), in comparison with the no turbulence case.

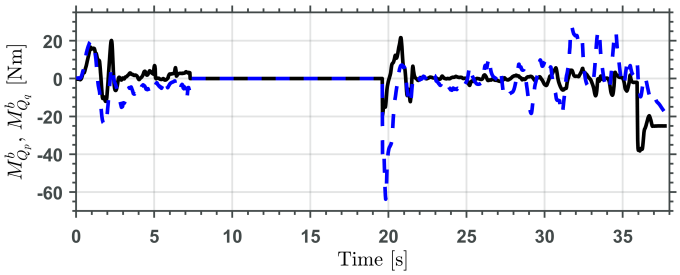

Figure 7: Angular moments calculated by $AAQC$ for the simulation with turbulence.

6 Conclusions

This work proposes an autopilot to assist a pilot in operating a hybrid aircraft known as a Quad-plane. The autopilot comprises four nonlinear control algorithms coordinated through a state machine. The autopilot is evaluated through a SITL co-simulation where the autopilot runs in MATLAB-Simulink while the aircraft dynamic model is simulated in X-Plane. Two simulations are reported. The first has optimal flight conditions, while the second considers turbulent conditions. The turbulence intensity was selected high enough to make

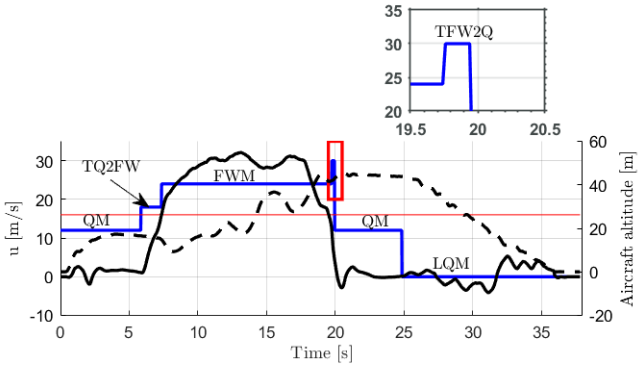

Figure 8: Quad-plane transitions, longitudinal and height speed for the simulation with turbulence.

the flight hard for the pilot. An important issue is left open in this work: the stability analysis of the complete closed-loop dynamic.

References

[1] L. Wang, X. Deng, J. Gui, P. Jiang, F. Zeng, and S. Wan, "A review of urban air mobility-enabled intelligent transportation systems: Mechanisms, applications and challenges," *Journal of Systems Architecture*, p. 102902, 2023.

[2] Q. Long, J. Ma, F. Jiang, and C. J. Webster, "Demand analysis in urban air mobility: A literature review," *Journal of Air Transport Management*, vol. 112, p. 102436, 2023.

[3] G. J. Ducard and M. Allenspach, "Review of designs and flight control techniques of hybrid and convertible vtol uavs," *Aerospace Science and Technology*, vol. 118, p. 107035, 2021.

[4] Wingtra, *A mapping drone for fast and accurate surveying data every time*, Accessed June 2024.

[5] K. Wang, Y. Ke, S. Lai, K. Gong, Y. Tan, and B. M. Chen, "Model-based optimal auto-transition and control synthesis for tail-sitter uav kh-lion," in *2017 13th IEEE International Conference on Control & Automation (ICCA)*, pp. 541–547, 2017.

[6] L. M. Sanchez-Rivera, R. Lozano, and A. Arias-Montano, "Transition flight dynamics of a dual tilt-wing uav," in *2020 International Conference on Unmanned Aircraft Systems (ICUAS)*, pp. 862–866, 2020.

[7] L. Zhou, J. Yang, T. Strampe, and U. Klingauf, "Incremental nonlinear dynamic inversion based path-following control for a hybrid quad-plane unmanned aerial vehicle," *International Journal of Robust and Nonlinear Control*, vol. 33, no. 17, pp. 10304–10327, 2023.

[8] A. Mathur and E. M. Atkins, "Design, modeling and hybrid control of a quadplane," in *AIAA Scitech 2021 Forum*, 2021.

[9] H. Zhao, Y. Xia, D. Ma, C. Hao, and F. Yu, "Active disturbance rejection altitude control for a quadplane," in *Advances in Guidance, Navigation and Control* (L. Yan, H. Duan, and X. Yu, eds.), (Singapore), pp. 329–342, Springer Singapore, 2022.

[10] T. T. Nguyen, D. Van Vu, S. X. Mai, and D. Thanh Nguyen, "An energy-effective altitude controller of a pusher-type hybrid uav in transition phases," in *2022 International Electrical Engineering Congress (iEECON)*, pp. 1–4, 2022.

[11] D. Van Vu, T. T. Nguyen, S. X. Mai, and D. T. Nguyen, "A robust transition control law for a quadplane," in *2022 International Conference on Electronics, Information, and Communication (ICEIC)*, pp. 1–4, 2022.

[12] H. Karssies and C. D. Wagter, "Extended incremental non-linear control allocation (xinca) for quadplanes," *International Journal of Micro Air Vehicles*, vol. 14, p. 17568293211070825, 2022.

[13] Z. Zyadat, N. Horri, M. Innocente, and T. Statheros, "Observer-based optimal control of a quadplane with active wind disturbance and actuator fault rejection," *Sensors*, vol. 23, no. 4, 2023.

[14] A. Astolfi, D. Karagiannis, and R. Ortega, *Nonlinear and Adaptive Control with Applications*, vol. 187. Springer, 2008.

[15] D. A. Martinez-Velasco, M. A. Martinez-Ramirez, and H. Rodriguez-Cortes, "Autopilot for flight mode transistion in quadplanes," *Memorias del Congreso Nacional de Control Automático*, vol. 6, pp. 568–573, 2023.

[16] E. A. Morelli and V. Klein, *Aircraft system identification: theory and practice*, vol. 2. Sunflyte Enterprises Williamsburg, VA, 2016.

[17] T. Lee, M. Leok, and N. H. McClamroch, "Global formulations of lagrangian and hamiltonian dynamics on manifolds," *Springer*, vol. 13, p. 31, 2017.

[18] E. M. Coates and T. I. Fossen, "Geometric reduced-attitude control of fixed-wing uavs," *Applied Sciences*, vol. 11, no. 7, 2021.

[19] J. L. Mendoza-Soto, J. J. Corona-Sánchez, and H. Rodríguez-Cortés, "Quadcopter path following control. a maneuvering approach," *Journal of Intelligent & Robotic Systems*, vol. 93, pp. 73–84, 2019.

[20] A. Lambregts, "Functional integration of vertical flight path and speed control using energy principles," *NASA. Langley Research Center NASA Aircraft Controls Research, 1983*, 1984.

[21] J. Brigido-González and H. Rodríguez-Cortés, "Experimental validation of an adaptive total energy control system strategy for the longitudinal dynamics of a fixed-wing aircraft," *Journal of Aerospace Engineering*, vol. 29, no. 1, p. 04015024, 2016.

[22] M. Sipser, *Introduction to the Theory of Computation*, vol. 27. ACM New York, NY, USA, 1996.

[23] P. Thomas, *X-Plane Blockset*. MATLAB Central File Exchange, Retrieved February 25, 2022.

[24] N. H. McClamroch, *Steady Aircraft Flight and Performance*. Princeton University Press, 2011.